Nano Research
2023, 16(9): 11839–11845

ISSN 1998-0124 CN 11-5974/O4
https://doi.org/10.1007/s12274-022-5230-5

Research Article

Synthesis and enhanced piezoelectric response of CVD-grown SnSe layered nanosheets for flexible nanogenerators

Fumei Yang, Man-Chung Wong, Jianfeng Mao, Zehan Wu, and Jianhua Hao (✉)

Department of Applied Physics, the Hong Kong Polytechnic University, Hong Kong 999077, China

Received: 14 September 2022 / **Revised:** 19 October 2022 / **Accepted:** 19 October 2022

ABSTRACT

Piezoelectricity is the electric charge which accumulates in certain materials in response to mechanical stimuli, while piezoelectric nanogenerators (PENGs) converting mechanical energy into electricity can be widely used for energy harvesting and self-powered systems. The group IV-VI monochalcogenides may exhibit strong piezoelectricity because of their puckered C_{2v} symmetry and electronic structure, making them promising for flexible PENG. Herein, we investigated the synthesis and piezoelectric properties of multilayer SnSe nanosheets grown by chemical vapor deposition (CVD). The SnSe nanosheets exhibited high single-crystallinity, large area, and good stability. The strong layer-dependent in-plane piezoelectric coefficient of SnSe nanosheets showed a saturated trend to be ~ 110 pm/V, which overcomes the weak piezoelectric response or odd-even effects in other layered nanosheets. A high energy conversion efficiency of 9.3% and a maximum power density of 538 mW/cm^2 at 1.03% strain have been demonstrated in a SnSe-based PENG. Based on the enhanced piezoelectricity of SnSe and attractive output performance of the nanogenerator, a self-powered sensor for human motion monitoring is further developed. These results demonstrate the strong piezoelectricity in high quality CVD-grown SnSe nanosheets, allowing for application in flexible smart piezoelectric sensors and advanced microelectromechanical devices.

KEYWORDS

SnSe, piezotronics, piezoresponse force microscope, piezoelectric nanogenerator, self-powered device

1 Introduction

Piezotronics coined by Professor Zhong Lin Wang play a core role in the field of functional sensors, wearable electronics, and microelectromechanical systems [1–3]. These applications rely on the strain-induced piezoelectric potential from the piezoelectric semiconductors as the gate controlling signal to tune the charge transport effectively [4–6]. Recently, two-dimensional (2D) materials have emerged as the promising candidate for flexible piezotronics taking advantage of their atomic-scale thickness, superior mechanical flexibility, and piezoelectric functionalities [2, 7]. The density-functional analysis suggests that 2D materials exhibit stronger piezoelectric coupling than some conventional piezoelectric bulk wurtzite structures, such as α-quartz, wurtzite GaN, and AlN [8–10]. Since the research groups of Wang and Zhang first experimentally investigated the intrinsic piezoelectric properties in monolayer MoS_2 [1, 11], considerable efforts have been devoted to exploring the piezoelectric properties of 2D semiconductors, including hexagonal boron nitride (h-BN), transition metal dichalcogenides (TMDs), group III and IV monochalcogenides [9, 12–14]. As for many layered materials like TMDs, the intrinsic in-plane piezoelectricity only presents in their monolayer or few-odd layers rather than even multilayers or bulk counterparts due to the cancellation of the induced polarization between the adjacent layers [1, 11]. Unfortunately, this odd-even effect and their low intrinsic piezoelectric in monolayer with poor mechanical durability may hinder their further applications [15]. To address these problems, a series of research has been done to induce symmetric breaking and improve their piezoelectric response, such as constructing Janus structure, utilizing novel stacking configurations, and passivating defects [15–20]. Despite the enhancement of piezoresponse through these engineering strategies, the output performance of the piezoelectric nanogenerators (PENGs) could only reach tens of millivolts and picoampere, indicating the limitation to achieve high conversion efficiency. Besides, the complicated and uncontrollable engineering process makes them less competitive for extensive practical applications.

Remarkably, group IV-VI monochalcogenides (MX, M = Sn or Ge, X = Se or S) are proposed to intrinsically exhibit significant piezoelectric coefficients (d_{11} = 75.43–250.58 pm/V), which show great potential in practical piezotronic applications to achieve high energy conversion efficiency [10]. Their puckered C_{2v} symmetries with flexible bonding along the armchair contribute to the significant enhancement in the magnitude of the in-plane piezoelectric coefficient [10]. SnSe with intriguing electrical and mechanical properties has aroused significant interest for piezotronic applications [10, 21, 22]. The SnSe film fabricated by mechanical exfoliation and SnSe nanowall/microspheres prepared by solution-mediated technique were developed into PENGs for self-powered pH sensors and finger force monitors, respectively [23, 24]. However, the SnSe samples synthesized by the above methods are limited in lateral size and surface roughness. In particular, the mechanical exfoliation method fails to achieve good controllability over size and lacks of scalability [25]. And although

Address correspondence to jh.hao@polyu.edu.hk

the one-pot solution mediated growth technique demonstrates tunability in shape and length, it fails to achieve uniform surface, which is important for carrier transport in piezotronic semicondutors [26]. In contrast, chemical vapor deposition (CVD) method has advantages in scalability, controllability, and mass production, allowing to obtain high crystalline quality and large area single-crystalline 2D materials [18, 25, 27, 28].

Here, we systematically investigated the intrinsically strong in-plane piezoelectric properties of CVD-grown multilayer SnSe nanosheets with different thickness via piezoreponse force microscope (PFM) technique. The as-prepared SnSe nanosheets demonstrate large area and good uniformity, which contribute to a low interface scattering across the whole nanosheets [25]. The effective piezoelectric coefficient d_{11} tends to be saturated to be ~ 110 pm/V. The SnSe nanosheet was further developed into a flexible PENG, demonstrating high piezoelectric output signals and good stability. In addition, the SnSe-based PENG was further demonstrated as a self-powered sensor to monitoring human motions. This work confirms the strong piezoelectricty of CVD-grown SnSe nanosheets and paves the avenue for the realization of novel high-performance nanogenerators and self-powered smart sensors.

2 Results and discussion

2.1 Synthesis and characterization of SnSe nanosheets

2D SnSe is an IV-VI monochalcogenide with orthorhombic structure composed of strong Sn–Se bonding in puckered layer, as depicted in Fig. 1(a). SnSe belongs to the *Pnma* (No. 62) symmetry group with low symmetry at ambient conditions [29]. In this investigation, the SnSe nanosheets were grown on mica substrates via CVD technique (see the Experimental section and Fig. S1 in Electronic Supplementary Material (ESM)). Figure 1(b) demonstrates the typical optical microscope image of the as-grown orthorhombic SnSe nanosheets with a lateral dimension of ~ 5–15 μm. The samples with different lateral dimensions and thicknesses could also be feasibly obtained by carefully adjusting the growth condition (See Figs. S2 and S3 in the ESM) [30]. The uniform contrast in Fig. 1(b) and the image of scanning electron microscopy (SEM, Fig. 1(c)) suggest their flatness of their surface and uniform thickness across the whole nanosheets. The corresponding energy-dispersive X-ray (EDX) elemental mapping images in the insets of Fig. 1(c) reveal the uniform chemical distribution and homogeneous chemical composition in SnSe nanosheets. Quantitative elemental analysis of EDX spectrum (Fig. S4 in the ESM) shows that the atomic ratio of Sn and Se is approximately 1:1, which matches well with the stoichiometric composition of SnSe. Raman spectroscopy and second harmonic generation (SHG) measurement were used to confirm the vibrational energy modes and the symmetry variations of SnSe. As shown in Fig. 1(d), four sharp Raman peaks located at ~ 70, ~ 102, ~ 125, and ~ 150 cm^{-1} were attributed A_g^1, B_{3g}, A_g^2, and A_g^3, respectively, which match well with the previous study [31]. A sharp SHG peak located at 450 nm under 900 nm laser excitation indicates SnSe was intrinsic non-centrosymmetric, showing potential for piezoelectric applications (inset of Fig. 1(e)). The uniform SHG mapping in Fig. 1(e) also demonstrates the high crystalline quality and uniformity of SnSe nanosheet. The microscopic structure of SnSe nanosheets was further confirmed by high resolution transmission electron microscopy (HRTEM) and selected area electron diffraction (SAED) (Figs. 1(f) and 1(g)), showing clear orthogonal lattice fringes, which suggests that the as-prepared SnSe nanosheets were single crystalline with high crystal quality. The lattice spacing along (011) and (0$\bar{1}$1) directions is ~ 3.0 Å, and their intersection angle is measured to be ~ 93°, which are consistent with the previously reported values [32, 33].

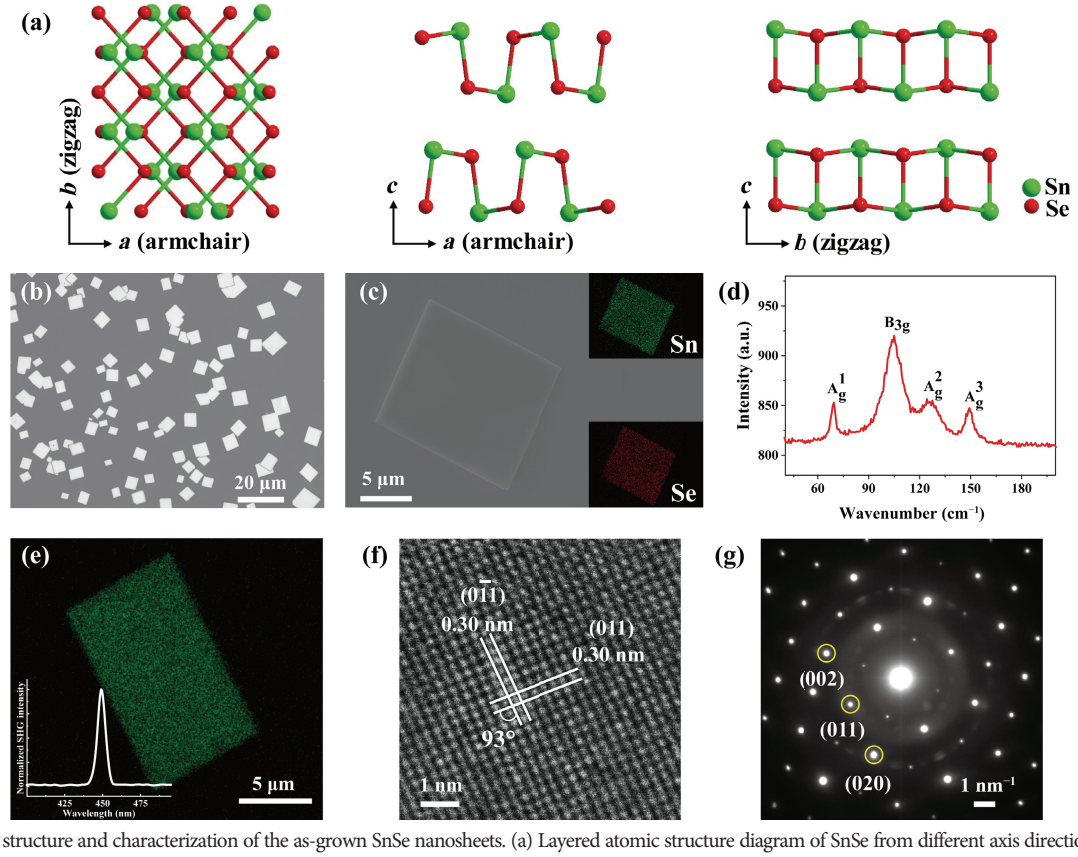

Figure 1 The structure and characterization of the as-grown SnSe nanosheets. (a) Layered atomic structure diagram of SnSe from different axis directions. (b) Typical optical microscope image of CVD-grown SnSe nanosheets on mica substrate. (c) SEM image of a typical SnSe nanosheet. Inset: EDX elemental mapping of Sn (green) and Se (red). (d) Raman spectrum. (e) SHG mapping. Inset: SHG spectrum. (f) High-resolution TEM image. (g) The corresponding SAED pattern.

These morphology and structural characterization results demonstrate SnSe nanosheets grown by CVD method exhibit uniform morphology and single-crystalline nature.

2.2 Layer-dependence in-plane piezoelectric properties of SnSe nanosheets

To investigate the intrinsic piezoelectricity of CVD-grown SnSe layered nanosheets, two typical SnSe nanosheets were selected to explore the in-plane piezoelectric response via PFM measurements. The schematic of the PFM system is shown in Fig. S5 in the ESM and the details of PFM measurements were described in the Experimental section and Note S1 in the ESM. The CVD-grown monolayer MoS_2 was used to calibrate the system (Figs. S6 and S7 in the ESM). The atomic force microscopy (AFM) results in in Fig. 2(a) show their heights were ~ 14 and ~ 27 nm, respectively. Figure 2(b) displays the lateral amplitude signals under different drive voltages ranging from 1.5 to 3 V. The strong lateral amplitudes from the SnSe nanosheets confirm the induced piezoresponse originating from SnSe samples rather than the substrate with negligible signals. The sharp piezoelectric contrast between SnSe nanosheets and substrate indicates the inherently robust in-plane piezoresponse of SnSe nanosheets. The piezoresponse of SnSe nanosheets with different thicknesses ranging from 10 to 120 nm is also given in Figs. S8–S10 in the ESM. It can be found that the lateral PFM amplitudes increased linearly with the increasing drive voltages, from which the effective in-plane piezoelectric coefficient d_{11} of SnSe nanosheets with different thicknesses could be deduced based on the slope (Fig. 2(c) and Figs. S8–S10 in the ESM). For relatively thin SnSe nanosheets, the d_{11} sequentially increases with the thickness, indicating a gradually increasing piezoresponse as the thickness increases. The comparison of experimentally confirmed in-plane piezoelectric coefficient among various layered piezoelectric materials is demonstrated in Fig. S11 in the ESM. The piezoreponse of 10 nm SnSe nanosheet (d_{11} = ~ 45.82 pm/V) is nearly twice larger than that of monolayer SnS (26.1 ± 0.3 pm/V) in the same group IV-VI monochalcogenides, and it is at least one order larger than that of monolayer MoS_2 (3.78 pm/V) and WSe_2 (3.26 ± 0.3 pm/V) [15, 34], suggesting SnSe is a competitive piezoelectric 2D material for practical applications. Taking advantages of flat surface and large area, the in-plane piezoresponse of CVD-grown SnSe nanosheets is at least twice larger than that of mechanical-exfoliated SnSe film (~ 23 pm/V) and $Sn_{1-x}Se_x$ nanowall/μ-spheres (19.9 and 6.8 pm/V, respectively) [23, 24]. As for the relatively thick samples, the d_{11} tends to be saturated at ~ 110 pm/V. The increase of piezoresponse with thickness in SnSe nanosheets attributes to reduced constraint derived from substrate clamping, which decreases with thickness and becomes negligible for thick nanosheets. This phenomenon is also discovered in several layered piezoelectric and ferroelectric materials, such as α-In_2Se_3, $Pb[Zr_xTi_{1-x}]O_3$ (PZT) films, and $CuInP_2S_6$ flakes [35–37]. The piezoelectric enhancement of SnSe originates from the unique "puckered" C_{2v} symmetry and intrinsic electronic structure of group IV monochalcogenides, which possess much smaller elastic stiffnesses for both clamped and relaxion cases than the typical D_{3h} symmetry piezoelectric materials with stronger covalence bonds [10]. These lateral PFM results confirmed the strong piezoresponse in CVD-grown layered SnSe nanosheets and demonstrated the great potential for practical piezoelectronic applications.

2.3 Piezotronic effect

The CVD-grown SnSe nanosheet was developed into a flexible piezoelectric nanogenerator device (SnSe-PENG) for piezoelectric output measurements. The SnSe sample was transferred onto 5/50 nm Ti/Au electrodes deposited on a flexible polyimide (PI) substrate. Detailed preparation process and the calculation of the strain are described in the Experimental section and Figs. S12–S14 and Notes S2–S3 in the ESM. The SnSe device can be feasibly bent into an arc shape, exhibiting good flexibility and allowing for applying mechanical force (Fig. 3(a)). Figure 3(b) demonstrates the optical microscope image of the device and the thickness of SnSe is ~ 60 nm. The device was fixed to a holder for applying the uniaxial strain (Fig. S14 in the ESM) for the direct-current electrical characterization. As shown in Fig. 3(c), the *I*–*V* curves of the SnSe piezoelectric device shift upward and downward with increased compressive and tensile strain, respectively. The electrical measurement results show that both metal–semiconductor junctions in this device are Schottky contacts. Under the uniaxial strains, the asymmetric variation of the current at −1 and 1 V originates from the piezotronic effect in SnSe, which is similar to that of the previously reported layered materials, such as MoS_2 and black phosphors (BP) [1, 38]. In detail, when the uniaxial strain was applied, the Sn–Se bonds would be elongated accordingly owing to the intrinsic non-centrosymmetric deformation (Fig. 3(d)), resulting in a piezoelectric dipole and field [1, 34]. Similar to BP with the

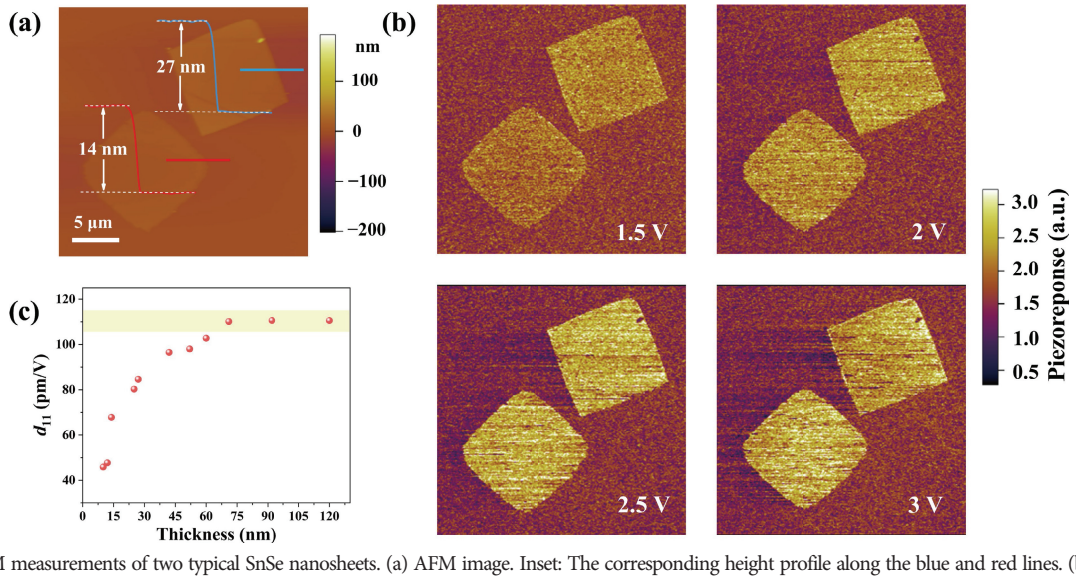

Figure 2 PFM measurements of two typical SnSe nanosheets. (a) AFM image. Inset: The corresponding height profile along the blue and red lines. (b) Lateral PFM amplitude images of two SnSe nanosheets under different drive voltages. (c) Piezoelectric coefficient of SnSe nanosheets with different thicknesses.

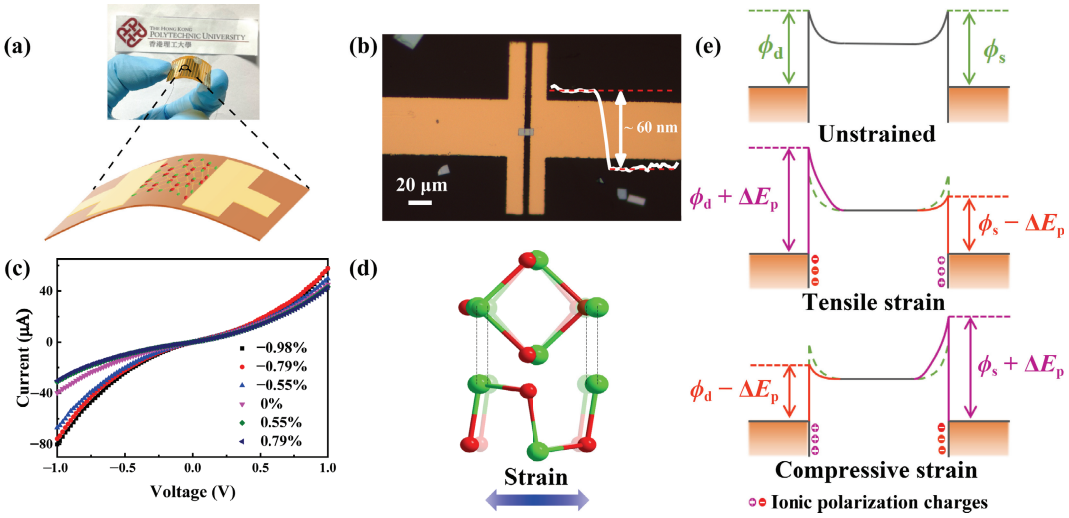

Figure 3 Flexible SnSe piezoelectric device and the direct-current electrical characterization. (a) Schematic of flexible SnSe device. (b) Optical microscope image of multilayer SnSe device. The thickness of the sample is about 60 nm (inset). Length: 6 μm. Width: 6.65 μm. (c) The asymmetric modulation of carrier transport by strains shows characteristics of a piezotronic effect. (d) Atomic structures for SnSe strained by an external stress. (e) Band diagrams of piezotronic behavior in SnSe. ϕ_d and ϕ_s stand for the Schottky barrier heights at drain and source contacts, respectively. ΔE_p indicates the change of the Schottky barrier height by piezoelectric polarization charges.

puckered structure, the piezoelectricity exists both in the odd and even layers despite the possible offsets between adjacent layers [38]. The puckered symmetries of SnSe make it more flexible than the ordinary 2D materials [10]. The band diagrams of piezotronic behavior are illustrated in Fig. 3(e). During the lattice deformation process, the piezoelectric polarization charges are accumulated in the Schottky contacts. The strain-induced negative polarization charges repel the electrons away from the interface, which induces a further depleted interface and results in an increased Schottky barrier height (SBH). While for the positive polarization charges, they attract the electrons toward the interface, which induces a less depleted interface, leading to a decreased SBH [2]. Therefore, an asymmetric SBH occurs at the source and drain, resulting in an asymmetric current variation in the SnSe device [1]. The SnSe nanosheet behaves similar to a control gate of a transistor where the carrier transport could be asymmetrically manipulated by the piezoelectric potential [39]. Besides, the obtained large current value also indicates a good contact between the SnSe flake and electrodes. The prominent piezotronic behavior in SnSe nanosheets manifests the superiority for practical flexible piezoelectric devices.

2.4 Performance of the piezoelectric nanogenerator and sensor for human motion monitoring

Due to the superb flexibility and strong piezoelectricity, SnSe nanosheets enable to be developed as piezoelectric nanogenerators for mechanical energy harvesting and flexible self-powered piezoelectric sensors. The piezoelectric nanogenerator based on SnSe nanosheets (SnSe-PENG) was first fabricated to measure the piezoelectric output performance. A linear mechanical system provided periodic strains to SnSe-PENG for piezoelectric output measurements (Fig. S15 in the ESM). The details of the test system and electrical measurements are described in the Experimental section. Figures 4(a) and 4(b) display the piezoelectric output voltage and current signals of SnSe-PENG. The positive output signals could be obtained under the tensile strain. As the strain is released from the SnSe-PENG, the output voltage and current become negative correspondingly. The typical open-circuit voltage and short-circuit current of SnSe-PENG under the strain of 1.03% were ~ 270 mV and ~ 297 pA, respectively. The switched polarity test (Fig. S16 in the ESM) indicates that the output signals of SnSe-PENG were obtained from the CVD-grown SnSe rather than the noise from the system background. The output signals increased with increasing applied strains ranging from 0.67% to 1.03%, as shown in Fig. S17 in the ESM. Moreover, the peak output current was stable at 1.03% strain for 1,600 s (Fig. 4(c)), which confirmed the excellent mechanical stability of the high-quality CVD-grown SnSe nanosheet, allowing for practical applications in wearable electronics, implantable electronics, and self-powered sensors for long-term working conditions.

To quantify the output power of the circuit, different external load resistances were integrated into the circuit for output measurements. In Fig. 4(d), the initial voltage was almost zero and began to increase when the load resistance was 12 kΩ. The output current decreased gradually with increasing load resistance (Fig. 4(e)). The maximum output power reached up to ~ 21 pW at 10 MΩ under a strain of 1.03% as shown in Fig. 4(f). Table S1 in the ESM summarizes the output performance of PENG based on different 2D materials. The generated voltage and current of SnSe-PENG are at least twice larger than the PENGs based on previously reported 2D materials (Table S1 in the ESM), such as MoS_2, WSe_2, In_2Se_3, and SnS [15, 34, 40]. The significant enhancement can be attributed to the high single-crystallinity and smooth surface of these CVD growth thin films. As the effective area of the SnSe-PENG was ~ 39 μm^2, the power density could reach up to ~ 538 mW/m^2, which is at least one order larger than the piezoelectric nanogenerators based on monolayer MoS_2, 48 nm 3R-MoS_2, SnS, and SnSe synthesized by the mechanical exfoliation method [1, 23, 40, 41]. The energy conversion efficiency is estimated to be ~ 9.3% (Note S4 in the ESM), which is significantly higher than those of PENGs based on MoS_2, WSe_2, and the mechanical-exfoliated SnSe film [1, 15, 23]. The superior performance of the SnSe-PENG mainly benefits from the high-quality CVD-grown SnSe nanosheet with high single-crystallinity and good surface roughness, allowing for efficient carrier transportation in the device. The high single crystallinity of CVD-grown SnSe nanosheets enables to suppress carrier scattering, usually induced by grain boundaries in polycrystals [25]. The prominent piezoelectric response endows the CVD-grown SnSe nanosheets to be suitable for practical applications in wearable electronics and energy harvesting devices.

Based on the excellent piezoelectric output performance, the flexible and wearable SnSe-PENG device was further attached to the finger and wrist of the tester to verify the potential of

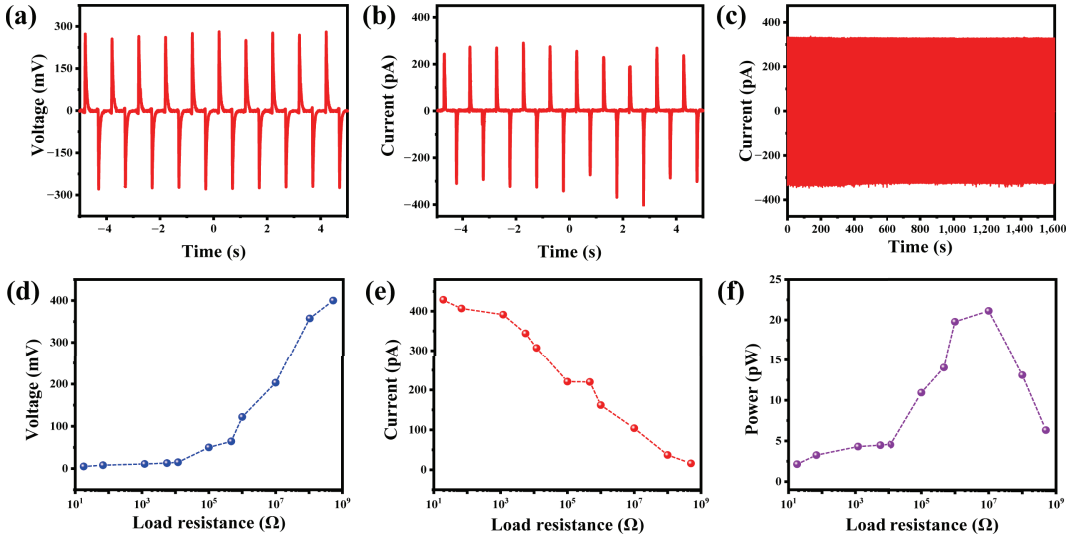

Figure 4 The output performance of piezoelectric nanogenerator based on CVD-grown SnSe. (a) Open-circuit voltage signals. (b) Short-circuit current signals. (c) Cyclic durability test for 1,600 s (1 s for 1 round). (d)–(f) The piezoelectric peak output voltage, current, and the corresponding power as a function of external load resistance at 1.03% strain, respectively.

displaying self-powered motion monitoring, as shown in Figs. 5(a) and 5(d). It can be observed that the positive and negative piezoelectric signals could be recorded without external bias at bending and releasing status, respectively. During the finger bending period, the recorded piezoelectric output voltage and current peaks are about 0.5 mV and 2.5 pA, respectively (Figs. 5(b) and 5(c)). The peak output voltage and current under wrist bending can reach about 1 mV and 4 pA, respectively (Figs. 5(e) and 5(f)). These piezoelectric output signals indicate that the SnSe sensor successfully converted the mechanical energy from the bending into electrical signals without power supply, which manifests its good self-powered sensing capability for human motion monitoring. These results suggest that the SnSe-PENG could effectively perform as a motion sensor for self-powered health-tracking wearable devices.

3 Conclusions

In summary, we have synthesized SnSe layered nanosheets by CVD method. The synthesis process and layered structure properties were studied. The piezoelectricity of CVD-grown multilayer SnSe nanosheets has been systematically investigated by analyzing the non-centrosymmetric lattice, observing the in-plane piezoelectric response and piezotronic effect, and recording the piezoelectric output signals in the piezoelectric devices for effective mechanical-to-electrical energy conversion and motion monitoring. The high conversion efficiency (~ 9.3%) of SnSe-PENG is attributed to the intrinsically large d_{11} and good sample quality, which benefits from the controllable CVD synthesis technique. These results suggest that CVD-grown SnSe nanosheets with strong piezoresponse present superior opportunities for applications in mechanical energy harvesting and self-powered electromechanical sensing systems.

4 Experimental section

4.1 Material growth

The SnSe nanosheets were synthesized on freshly-cleaved fluorphlogopite mica (1.2 cm × 1.2 cm) via the CVD method. A schematic of the CVD setup was shown in Fig. S1 in the ESM. SnSe (99.999%, Alfa Aesar) powders as the precursor were loaded in a quartz boat and placed in the center of the furnace. The mica substrates were put at the downstream of the furnace with a distance of 10–12.4 cm to the center of the furnace. Before the growth, the pressure of the quartz tube was first decreased to about 1×10^{-2} Pa. Afterwards, the quartz tube was flushed with N_2 to remove the air until the atmospheric pressure was achieved. 50 sccm N_2 was then introduced as the carrier gas. During the growth process, the furnace was heated to 670–750 °C in 30 min and then kept for 3–5 min. The temperature gradient at different positions of the substrates at the furnace downstream (~ 5 °C/cm) was measured by an electrical thermometer. The SnSe nanosheets could be deposited by selenization of Sn at a temperature gradient ranging from 540 to 570 °C at the downstream of the furnace [42]. After the growth time, the furnace was naturally cooled to room temperature. The SnSe nanosheets were flatly grown on the mica substrate at the downstream of the furnace.

4.2 Material characterization

The morphology and structure were examined by optical microscope (LEICA DM2700 M), SEM (JEOL 6490), and TEM (JEOL 2100F). The optical properties of SnSe nanosheets were investigated by Raman spectroscopy (532 nm, Witec Confocal Raman system) and SHG (Leica TCS SP8 MP system). The thickness of the samples was confirmed by AFM (standard mode, Asylum MFP 3D Infinity).

4.3 In-plane PFM measurement

The piezoelectric properties of SnSe nanosheets were confirmed by Asylum MFP 3D Infinity operating in vector piezoresponse force microscopy (vector PFM) mode with a conductive and Pt/Ir coated tip with a spring constant of 0.1–0.2 N/m (Bruker, SCM-PIC-V2). The details of the PFM measurement were explained in Note S1 in the ESM.

4.4 Device fabrication

The SnSe-PENG device was prepared by patterning 5/50 nm Ti/Au electrodes via standard photolithography followed by an electron-beam evaporation and a lift-off process. The SnSe nanosheets were first transferred onto SiO_2/Si substrate by the wet transfer process (Fig. S12 in the ESM) and then transferred onto electrodes by a dry transfer platform (Fig. S13 in the ESM). Finally, two copper wires were connected to the source and drain electrodes via silver paste. The piezotronic effect of SnSe nanosheets was confirmed using a probe station equipped with Keithley 4200-SCS semiconductor parameter analyzer. The

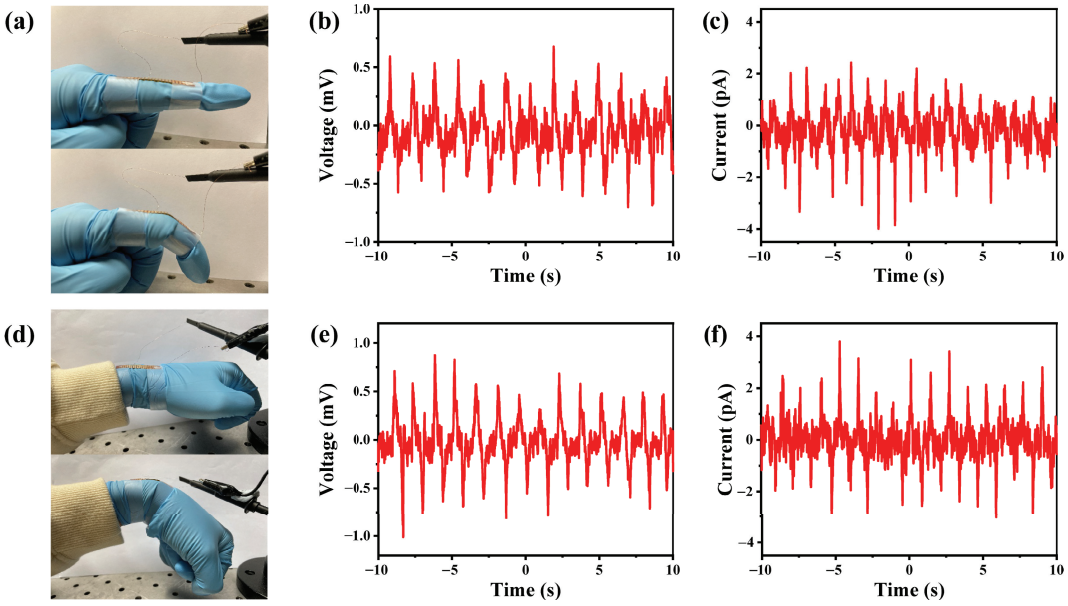

Figure 5 Self-powered piezoelectric sensor based on CVD-grown SnSe nanosheet. (a) Finger motion monitoring while being released and bent. (b) and (c) The corresponding output voltage and current obtained from finger motion. (d) Wrist motion monitoring while being released and bent. (e) and (f) The corresponding output voltage and current obtained from wrist motion.

uniaxial strain was applied by a home-made fixing stage (Fig. S14(a) in the ESM). The schematic of the original status and bending status were demonstrated in Figs. S14(b) and S14(c) in the ESM, and the calculation of strains was provided in Note S3 in the ESM.

4.5 Piezoelectric output performance measurements

A home-made system was set up to provide cyclic bending on the SnSe-PENG device (Fig. S15 in the ESM). An oscillator (LeCroy WaveSurfer 62Xs) and low-noise current preamplifier (Stanford Research Systems Model SR570) were employed to measure the piezoelectric output signals of SnSe-PENG.

Acknowledgements

This work was supported by the grants from Research Grants Council of Hong Kong (Nos. GRF PolyU 153025/19P, SRFS2122-5S02, and AoE/P-701/20) and PolyU Otto Poon Charitable Foundation Research Institute for Smart Energy (No. Q-CDBD).

Electronic Supplementary Material: Supplementary material (further details of growth results, PFM measurement, device fabrication and output performance measurements, calculation of applied strain, energy conversion efficiency of SnSe-PENG, and comparison of experimental results of different 2D materials) is available in the online version of this article at https://doi.org/10.1007/s12274-022-5230-5.

References

[1] Wu, W. Z.; Wang, L.; Li, Y. L.; Zhang, F.; Lin, L.; Niu, S. M.; Chenet, D. L.; Zhang, X.; Hao, Y. F.; Heinz, T. F. et al. Piezoelectricity of single-atomic-layer MoS_2 for energy conversion and piezotronics. *Nature* **2014**, *514*, 470–474.

[2] Wu, W. Z.; Wang, Z. L. Piezotronics and piezo-phototronics for adaptive electronics and optoelectronics. *Nat. Rev. Mater.* **2016**, *1*, 16031.

[3] Wang, Z. L. Progress in piezotronics and piezo-phototronics. *Adv. Mater.* **2012**, *24*, 4632–4646.

[4] Wang, Z. L.; Song, J. H. Piezoelectric nanogenerators based on zinc oxide nanowire arrays. *Science* **2006**, *312*, 242–246.

[5] Zhang, Y.; Liu, Y.; Wang, Z. L. Fundamental theory of piezotronics. *Adv. Mater.* **2011**, *23*, 3004–3013.

[6] Wang, Z. L. Towards self-powered nanosystems: From nanogenerators to nanopiezotronics. *Adv. Funct. Mater.* **2008**, *18*, 3553–3567.

[7] Han, S. A.; Lee, J.; Lin, J. J.; Kim, S. W.; Kim, J. H. Piezo/triboelectric nanogenerators based on 2-dimensional layered structure materials. *Nano Energy* **2019**, *57*, 680–691.

[8] Duerloo, K. A. N.; Ong, M. T.; Reed, E. J. Intrinsic piezoelectricity in two-dimensional materials. *J. Phys. Chem. Lett.* **2012**, *3*, 2871–2876.

[9] Blonsky, M. N.; Zhuang, H. L.; Singh, A. K.; Hennig, R. G. *Ab initio* prediction of piezoelectricity in two-dimensional materials. *ACS Nano* **2015**, *9*, 9885–9891.

[10] Fei, R. X.; Li, W. B.; Li, J.; Yang, L. Giant piezoelectricity of monolayer group IV monochalcogenides: SnSe, SnS, GeSe, and GeS. *Appl. Phys. Lett.* **2015**, *107*, 173104.

[11] Zhu, H. Y.; Wang, Y.; Xiao, J.; Liu, M.; Xiong, S. M.; Wong, Z. J.; Ye, Z. L.; Ye, Y.; Yin, X. B.; Zhang, X. Observation of piezoelectricity in free-standing monolayer MoS_2. *Nat. Nanotechnol.* **2015**, *10*, 151–155.

[12] Hinchet, R.; Khan, U.; Falconi, C.; Kim, S. W. Piezoelectric properties in two-dimensional materials: Simulations and experiments. *Mater. Today* **2018**, *21*, 611–630.

[13] Li, W. B.; Li, J. Piezoelectricity in two-dimensional group-III monochalcogenides. *Nano Res.* **2015**, *8*, 3796–3802.

[14] Lee, G. J.; Lee, M. K.; Park, J. J.; Hyeon, D. Y.; Jeong, C. K.; Park, K. I. Piezoelectric energy harvesting from two-dimensional boron nitride nanoflakes. *ACS Appl. Mater. Interfaces* **2019**, *11*, 37920–37926.

[15] Lee, J. H.; Park, J. Y.; Cho, E. B.; Kim, T. Y.; Han, S. A.; Kim, T. H.; Liu, Y. N.; Kim, S. K.; Roh, C. J.; Yoon, H. J. et al. Reliable piezoelectricity in bilayer WSe_2 for piezoelectric nanogenerators. *Adv. Mater.* **2017**, *29*, 1606667.

[16] Lu, A. Y.; Zhu, H. Y.; Xiao, J.; Chuu, C. P.; Han, Y. M.; Chiu, M. H.; Cheng, C. C.; Yang, C. W.; Wei, K. H.; Yang, Y. M. et al. Janus monolayers of transition metal dichalcogenides. *Nat. Nanotechnol.* **2017**, *12*, 744–749.

[17] Yuan, S. G.; Io, W. F.; Mao, J. F.; Chen, Y. C.; Luo, X.; Hao, J. H. Enhanced piezoelectric response of layered In_2Se_3/MoS_2 nanosheet-based van der Waals heterostructures. *ACS Appl. Nano Mater.* **2020**, *3*, 11979–11986.

[18] Mao, J. F.; Wu, Z. H.; Guo, F.; Hao, J. H. Strain-induced performance enhancement of a monolayer photodetector via patterned substrate engineering. *ACS Appl. Mater. Interfaces* **2022**, *14*, 36052–36059.

[19] Han, S. A.; Kim, T. H.; Kim, S. K.; Lee, K. H.; Park, H. J.; Lee, J.

H.; Kim, S. W. Point-defect-passivated MoS_2 nanosheet-based high performance piezoelectric nanogenerator. *Adv. Mater.* **2018**, *30*, 1800342.

[20] Io, W. F.; Wong, M. C.; Pang, S. Y.; Zhao, Y. Q.; Ding, R.; Guo, F.; Hao, J. H. Strong piezoelectric response in layered $CuInP_2S_6$ nanosheets for piezoelectric nanogenerators. *Nano Energy* **2022**, *99*, 107371.

[21] Shi, W. R.; Gao, M. X.; Wei, J. P.; Gao, J. F.; Fan, C. W.; Ashalley, E.; Li, H. D.; Wang, Z. M. Tin selenide (SnSe): Growth, properties, and applications. *Adv. Sci.* **2018**, *5*, 1700602.

[22] Yang, S. X.; Liu, Y.; Wu, M. H.; Zhao, L. D.; Lin, Z. Y.; Cheng, H. C.; Wang, Y. L.; Jiang, C. B.; Wei, S. H.; Huang, L. et al. Highly-anisotropic optical and electrical properties in layered SnSe. *Nano Res.* **2018**, *11*, 554–564.

[23] Li, P.; Zhang, Z. K.; Shen, W. T.; Hu, C. G.; Shen, W. F.; Zhang, D. Z. A self-powered 2D-material sensor unit driven by a SnSe piezoelectric nanogenerator. *J. Mater. Chem. A* **2021**, *9*, 4716–4723.

[24] Alluri, N. R.; Raj, N. P. M. J.; Khandelwal, G.; Kim, S. J. Shape-dependent in-plane piezoelectric response of SnSe nanowall/microspheres. *Nano Energy* **2021**, *88*, 106231.

[25] Cai, Z. Y.; Liu, B. L.; Zou, X. L.; Cheng, H. M. Chemical vapor deposition growth and applications of two-dimensional materials and their heterostructures. *Chem. Rev.* **2018**, *118*, 6091–6133.

[26] Cui, C. J.; Xue, F.; Hu, W. J.; Li, L. J. Two-dimensional materials with piezoelectric and ferroelectric functionalities. *NPJ 2D Mater. Appl.* **2018**, *2*, 18.

[27] Lyu, Y.; Wu, Z. H.; Io, W. F.; Hao, J. H. Observation and theoretical analysis of near-infrared luminescence from CVD grown lanthanide Er doped monolayer MoS_2 triangles. *Appl. Phys. Lett.* **2019**, *115*, 153105.

[28] Io, W. F.; Yuan, S. G.; Pang, S. Y.; Wong, L. W.; Zhao, J.; Hao, J. H. Temperature- and thickness-dependence of robust out-of-plane ferroelectricity in CVD grown ultrathin van der Waals α-In_2Se_3 layers. *Nano Res.* **2020**, *13*, 1897–1902.

[29] Zhao, L. D.; Lo, S. H.; Zhang, Y. S.; Sun, H.; Tan, G. J.; Uher, C.; Wolverton, C.; Dravid, V. P.; Kanatzidis, M. G. Ultralow thermal conductivity and high thermoelectric figure of merit in SnSe crystals. *Nature* **2014**, *508*, 373–377.

[30] Zhao, S. L.; Wang, H.; Zhou, Y.; Liao, L.; Jiang, Y.; Yang, X.; Chen, G. C.; Lin, M.; Wang, Y.; Peng, H. L. et al. Controlled synthesis of single-crystal SnSe nanoplates. *Nano Res.* **2015**, *8*, 288–295.

[31] Chandrasekhar, H. R.; Humphreys, R. G.; Zwick, U.; Cardona, M. Infrared and Raman spectra of the IV-VI compounds SnS and SnSe. *Phys. Rev. B* **1977**, *15*, 2177–2183.

[32] Vaughn II, D. D.; In, S. I.; Schaak, R. E. A precursor-limited nanoparticle coalescence pathway for tuning the thickness of laterally-uniform colloidal nanosheets: The case of SnSe. *ACS Nano* **2011**, *5*, 8852–8860.

[33] Ma, X. H.; Cho, K. H.; Sung, Y. M. Growth mechanism of vertically aligned SnSe nanosheets via physical vapour deposition. *CrystEngComm* **2014**, *16*, 5080–5086.

[34] Kim, S. K.; Bhatia, R.; Kim, T. H.; Seol, D.; Kim, J. H.; Kim, H.; Seung, W.; Kim, Y.; Lee, Y. H.; Kim, S. W. Directional dependent piezoelectric effect in CVD grown monolayer MoS_2 for flexible piezoelectric nanogenerators. *Nano Energy* **2016**, *22*, 483–489.

[35] Xue, F.; Zhang, J. W.; Hu, W. J.; Hsu, W. T.; Han, A. L.; Leung, S. F.; Huang, J. K.; Wan, Y.; Liu, S. H.; Zhang, J. L. et al. Multidirection piezoelectricity in mono- and multilayered hexagonal α-In_2Se_3. *ACS Nano* **2018**, *12*, 4976–4983.

[36] Kim, D. M.; Eom, C. B.; Nagarajan, V.; Ouyang, J.; Ramesh, R.; Vaithyanathan, V.; Schlom, D. G. Thickness dependence of structural and piezoelectric properties of epitaxial $Pb(Zr_{0.52}Ti_{0.48})O_3$ films on Si and $SrTiO_3$ substrates. *Appl. Phys. Lett.* **2006**, *88*, 142904.

[37] Liu, F. C.; You, L.; Seyler, K. L.; Li, X. B.; Yu, P.; Lin, J. H.; Wang, X. W.; Zhou, J. D.; Wang, H.; He, H. Y. et al. Room-temperature ferroelectricity in $CuInP_2S_6$ ultrathin flakes. *Nat. Commun.* **2016**, *7*, 12357.

[38] Ma, W. D.; Lu, J. F.; Wan, B. S.; Peng, D. F.; Xu, Q.; Hu, G. F.; Peng, Y. Y.; Pan, C. F.; Wang, Z. L. Piezoelectricity in multilayer black phosphorus for piezotronics and nanogenerators. *Adv. Mater.* **2020**, *32*, 1905795.

[39] Zhou, J.; Fei, P.; Gu, Y. D.; Mai, W. J.; Gao, Y. F.; Yang, R. S.; Bao, G.; Wang, Z. L. Piezoelectric-potential-controlled polarity-reversible Schottky diodes and switches of ZnO wires. *Nano Lett.* **2008**, *8*, 3973–3977.

[40] Khan, H.; Mahmood, N.; Zavabeti, A.; Elbourne, A.; Rahman, A.; Zhang, B. Y.; Krishnamurthi, V.; Atkin, P.; Ghasemian, M. B.; Yang, J. et al. Liquid metal-based synthesis of high performance monolayer SnS piezoelectric nanogenerators. *Nat. Commun.* **2020**, *11*, 3449.

[41] Hallil, H.; Cai, W. F.; Zhang, K.; Yu, P.; Liu, S.; Xu, R.; Zhu, C.; Xiong, Q. H.; Liu, Z.; Zhang, Q. Strong piezoelectricity in 3R-MoS_2 flakes. *Adv. Electron. Mater.* **2022**, *8*, 2101131.

[42] Huang, Y.; Xu, K.; Wang, Z. X.; Shifa, T. A.; Wang, Q. S.; Wang, F.; Jiang, C.; He, J. Designing the shape evolution of $SnSe_2$ nanosheets and their optoelectronic properties. *Nanoscale* **2015**, *7*, 17375–17380.